Thermogravimetric Analysis of Synthesis Variation Effects on CVD Generated Multiwalled Carbon Nanotubes

Gregg S. B. McKee and Kenneth S. Vecchio*

Materials Science and Engineering Program, Jacobs School of Engineering, University of California, San Diego, La Jolla, California, 92093

Received: August 1, 2005; In Final Form: November 11, 2005

Changes in the thermogravimetrically determined oxidation behaviors of CVD-grown multiwalled carbon nanotubes with varying synthesis conditions are examined. Catalyst type and synthesis temperature are found to have a measurable impact upon nanotube stability, suggesting differing levels of crystalline perfection in the resulting nanotubes. The results provide evidence showing the catalytic effects of nanotube catalyst particles and their oxides upon the oxidation of nanotube carbon and graphite. The significance of thermogravimetric analysis as a characterization tool for carbon nanotubes is discussed.

Introduction

In the years following their identification,[1] carbon nanotubes (CNTs) have generated considerable interest in a variety of fields from electronics to hydrogen storage to high-strength composites.[2−5] Extraordinary properties such as high specific surface area, tunable electrical properties (semiconductor or conductor, depending upon chirality), and high specific strength and specific stiffness have been attributed to various forms of CNTs. However, to realize their full potential, a more complete understanding of synthesis, purification, and processing is required.

Thermogravimetric analysis (TGA) of nanotube oxidation has shown to be a useful technique for the characterization of CNTs.[6−9] Defects in nanotube walls increase the local reactivity, leading to a lower temperature oxidation and gasification of the carbon, and manifesting itself in the TGA mass-loss profile.

The oxidation of nanotubes has been of interest for the purposes of characterization and oxidative purification of raw CNT,[10−14] cap removal and subsequent nanotube filling for nanowire fabrication,[6,15−17] and for removal of CNT templates used in fabrication of other structures.[18] Various oxidizers have been examined in previous studies, including oxidation by acids,[16] other oxides,[11,17] and air, gaseous oxygen, or ozone,[7,11,14,19] with the objective of modeling nanotube oxidation chemistry.

Refinement of nanotubes involving the removal of nonnanotube carbon impurities such as amorphous carbon, other fullerenes, and graphite is possible through partial oxidation, but as it progresses simultaneously in a competitive manner among the various forms, only those less stable than nanotubes may be effectively removed in this manner. According to prior work,[7,8,14] amorphous carbon and fullerenes may be removed in this way, but there exists conflicting evidence with regard to graphite. Bom et al.[7] report the oxidative stability of graphite to be higher than that of multiwalled carbon nanotubes (MWNTs) tested, provided both are in the same state of annealing, but thermogravimetric analyses by Saxby et al.[20] and Pang et al.[8] suggest a decreased stability relative to nanotube forms of carbon. Significant work has also been done on the effects of transition metal catalysts upon the oxidation of graphite;[21] however, very little has been performed with respect to the helical forms of carbon.

In this paper, the thermogravimetric oxidation profiles of various forms of carbon and nanotube synthesis byproducts are compared to those of CNTs grown via chemical vapor deposition (CVD) with varying synthesis conditions in an attempt to further illuminate and optimize the generation of nanotubes and clarify the characteristics of their oxidation. The profiles are further compared with those obtained by several other research groups, and reasons are suggested for the differences. The effects of catalyst type on the temperatures and rates of oxidation are examined and comparisons drawn between their effects on graphite versus on CNTs.

Experimental Section

The carbon nanotubes examined in this study were prepared through the pyrolytic decomposition of benzene with an organometallic or metal chloride catalyst precursor in a CVD furnace as shown in Figure 1. Nanotube growth temperatures, catalyst precursors (ferrocene, nickelocene, cobaltocene, $NiCl_2$, $CoCl_2$), and carrier gas flow rate (low and high rates of flow) were varied during synthesis, as described in Table 1, to elucidate oxidative differences in the resulting nanotubes.

In the case of the low carrier gas flow rate experiments (herein referred to as "low-flow samples"), CNT synthesis began with the initiation of the argon carrier gas through the reaction chamber at the rate of approximately 90−280 sccm while the furnace heated to the set temperature. Once at temperature, a mixture of the carbon source and catalyst precursor was introduced. The solution was collected in a crucible inside the furnace tube and vaporized by the heat of the furnace. The vapor then entered the furnace, where nanotubes deposited onto a quartz substrate. Upon exhaustion of the feedstock solution, or after a designated period of time, the feedstock supply was halted (as necessary), the furnace shut down, and argon flow maintained until the chamber had completely cooled.

One variation on this method occurred in the generation of the amorphous carbon and nanotube combination sample (sample no. 1): instead of being mixed prior to introduction into the furnace, ferrocene was placed into the crucible inside the furnace and benzene dripped onto it. Similar to the process described previously, the evaporating vapors were then carried into the furnace. As this sample is used only to elucidate the

10.1021/jp054265h CCC: $33.50
Published on Web 12/31/2005

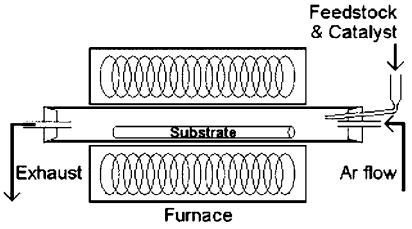

Figure 1. Schematic of complete CNT growth setup.

difference in reactivity between amorphous and nanotube carbon and not to structurally characterize the nanotubes, the significance of this variation should be negligible.

For high carrier gas flow rate experiments ("spray pyrolysis" samples), argon was again used as the carrier gas, but at a much higher flow rate (64 000−72 000 sccm ±5%). The furnace was brought to temperature and argon flow was initiated. A mixture of catalyst and carbon source was introduced into the high velocity argon stream, rapidly atomized, and carried into the furnace where nanotubes deposited. On completion of the run, the furnace was shut down and the argon flow lowered to rates used in the low-flow experiments while the furnace cooled to room temperature.

Upon conclusion of the growth process, mats of vertically aligned CNTs were removed from the quartz substrate and broken up into small chunks. Transmission (Philips EM420, 120 kV accelerating voltage) and scanning electron microscopies (Philips XL20, 15 kV accelerating voltage) were used to confirm the presence and alignment of multiwalled nanotubes (MWNTs), determine their diameter and length, and gauge the relative purity of the samples. Raman spectroscopy (Renishaw Raman) was performed at room temperature using approximately 0.347 mW (as measured at the sample) of 514.5 nm laser light from an Ar ion laser. X-ray diffraction (XRD; Rigaku D/Max RB, Cu Kα X-ray source), and transmission Mössbauer spectroscopy (^{57}Co in Rh source, iron metal calibration) were performed on several samples as well.

Mass-loss profiles were obtained by individually placing small (<10 mg) samples in open-top alumina sample pans in a Perkin-Elmer Diamond TG/DTA under a purge gas of 2% O_2, balance He. The temperature was raised to 200 °C and allowed to equilibrate for a period of 10 min before ramping to 1000 °C at the rate of 1 °C/min. The 1°/min heating rate was chosen to approximate the reaction equilibrium state and allow direct comparison between these data and those found in other works.[7,8,20]

To obtain a baseline for the comparison of the oxidation of nanotubes, a 99.9995% graphite sample (Alfa Aesar, 325 mesh) was examined. Similarly, mixtures of graphite and fine powders (200−325 mesh) of common nanotube catalysts such as iron (19.7 wt %, 200 mesh), cobalt (21.0 wt %, 270 mesh), nickel (19.9 wt %, 325 mesh by 0.37 μm thick), and their oxides (generated through oxidation of the powders), iron oxide (Fe_2O_3, 19.0 wt %), cobalt oxide (CoO and Co_3O_4, 20.0 wt %), and nickel oxide (NiO, 20.0 wt %) were prepared and analyzed. To enhance our capability to differentiate between forms of carbon, as well as other materials present, a homogeneous combination of amorphous and nanotube carbon (sample no. 1) and a heterogeneous mixture of graphite (1.44 mg) and nanotubes (0.78 mg, sample no. 4) were each profiled. In all cases of mass-loss profile determination, efforts were made to use samples with similar forms, consisting of multiple small segments (the exact number depending on sample size) of broken-up nanotube mats instead of larger macroscopic chunks of well-aligned nanotubes.

Results

As synthesized, the nanotubes ranged in diameter from ∼15 to ∼100 nm in any given sample and in length from several tens of microns to a few millimeters across all the samples. Sample purification was not undertaken as examination through electron microscopy showed most nanotube samples to be almost entirely nanotubes with little to no contamination with respect to other forms of carbon (Figures 2 and 3). In those cases where carbonaceous or metallic impurities were present, they were frequently detected through the TGA profile, as will be shown. Successive iterations with a given set of synthesis conditions resulted in similar quality nanotubes in terms of physical dimensions, morphology, and thermogravimetric oxidation mass-loss profile, so the results presented should be generally representative.

Graphite burnoff profiles as measured appear in Figure 4, and their corresponding burnoff rates appear in Figure 5. The high-purity graphite burns off completely with a maximum rate of burnoff occurring at approximately 850 °C, while the 20 wt % catalyst/graphite mixtures exhibited maximum rates at lower temperatures. The iron mixture exhibited the highest temperature of peak burnoff rate at 830 °C, followed by nickel at 800 °C, and cobalt at approximately 775 °C. Nickel oxide/graphite and cobalt oxide/graphite mixtures showed peak rates at approximately 805 and 785 °C, respectively, while iron oxide/graphite exhibited a maximum rate of oxidation just below 800 °C. In successive iterations, some variation was observed in the temperatures of peak oxidation rate, but the figures shown and temperatures quoted are indicative of the general trends observed.

The first sample of mixed carbon forms was initially thought to be solely amorphous carbon, caked onto the sides of the furnace tube. In Figure 6, however, there is a distinct two-stage burnoff, with one peak rate occurring at approximately 500 °C and a second occurring at 581 °C, suggesting a dual composition, later to be determined through comparison with other TGA results as well as XRD and transmission electron microscopy as amorphous carbon mixed with CNTs.

The profile for nanotubes mixed with high-purity graphite appears in Figure 7. Similar to Figure 6, a distinct two-stage burnoff is exhibited, with approximately 35% of the initial mass being lost in the first phase and the remainder in the second, corresponding very closely to the initial mix ratio. The points of peak burnoff rate occur at approximately 570 and 760 °C.

Burnoff profiles and rates were recorded (Figure 8) for four nanotube samples (samples 2−5), where only the furnace temperature was varied significantly during synthesis: 760, 800, 850, and 900 °C. Low-flow, ferrocene catalyzed nanotubes were used for this examination, as this combination of synthesis conditions resulted in relatively high yields of nanotubes. The oxidation of the lower synthesis temperature nanotubes begins slightly earlier than those synthesized at higher temperatures, but oxidation is complete at approximately the same temperature in all cases. This trend is evident in the oxidation rate results as well. All, except the 900 °C sample, appear to have a maximum rate at 590 °C, but for CNTs synthesized at 850 °C, initial oxidation is delayed in comparison to the other samples. Also, the nanotubes synthesized at 850 and 900 °C tend to have a more acute and rapid oxidation than those of lower synthesis temperatures. The rate chart also exhibits two peaks for most synthesis temperatures. A peak at approximately 560 °C is present, but secondary to the peak at 595 °C in the curves corresponding to 760 and 800 °C synthesis temperatures, resulting in a broadened burnoff peak. At 850 °C, the 560 °C

TABLE 1: Summary of the Synthesis Conditions for All Samples Used

sample	synthesis temp (°C)	purge gas flow rate	benzene vol (mL)	catalyst	where used
1	800	88.9 sccm, 99.5% Ar	excess	1.5 g of ferrocene	Figure 6
2	760	200 sccm, 99.5% Ar	10.0	0.75 g of ferrocene	Figures 8 and 11
3	800	95 sccm, 99.999% Ar	10.0	0.76 g of ferrocene	Figures 8, 9, and 11
4	850	280 sccm, 99.5% Ar	20.2	1.5 g of ferrocene	Figures 7, 8, and 11
5	900	200 sccm, 99.5% Ar	20.0	1.5 g of ferrocene	Figures 8 and 11
6	800	88.9 sccm, 99.5% Ar	10.0	0.75 g of nickelocene	Figures 9 and 11
7	800	91.2 sccm, 99.5% Ar	9.9	0.74 g of cobaltocene	Figures 9 and 11
8	850	70 000 sccm, 99.5% Ar	10.0	0.55 g of $NiCl_2$[a]	Figure 10
9	850	64 000 sccm, 99.5% Ar	5.0	0.55 g of $CoCl_2$[a]	Figure 10
10	850	72 000 sccm, 99.5% Ar	10.0	0.75 g of ferrocene	Figure 10

[a] In the case of samples 8 and 9, the metal chlorides were dissolved in 5.0 mL of methanol and then combined with benzene.

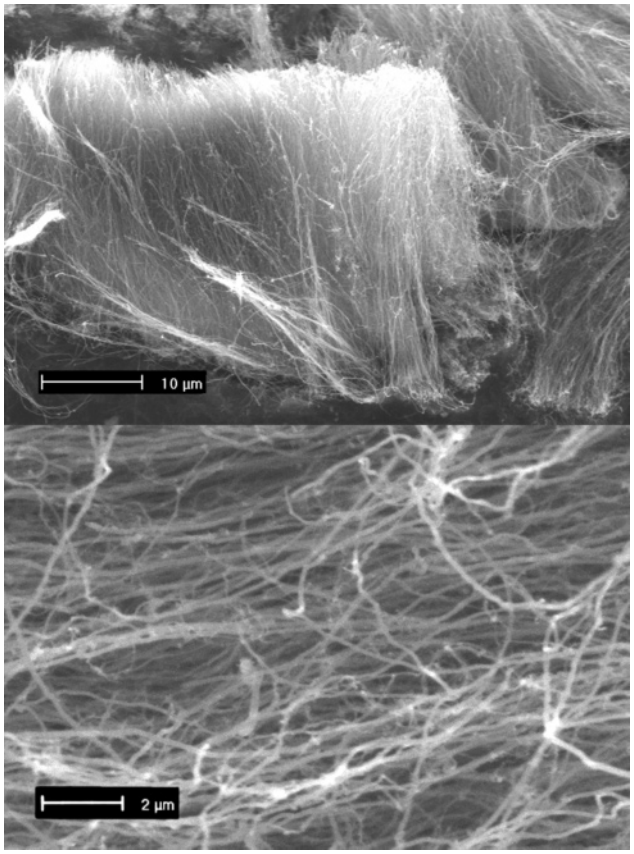

Figure 2. Scanning electron micrographs of CNTs. (top) Most nanotubes examined in this study were synthesized in preferentially aligned mats and appeared similar in form to those shown here. Scale bar = 10 μm. (bottom) Higher magnification image showing individual nanotubes. Scale bar = 2 μm.

peak is almost nonexistent. At 900 °C, however, the 595 °C peak is significantly diminished and the lower temperature peak dominates burnoff.

Burnoff profiles and rates for nanotubes generated by the low-flow method with varying catalyst types are shown in Figure 9, and those for nanotubes generated by the spray pyrolysis method, again with varying catalyst types, are shown in Figure 10. In general, nanotubes grown using the low-flow method show a higher carbon fraction than those grown through spray pyrolysis, resulting in a lower residual mass fraction at completion of burnoff. Catalyst particles are generally similar in size across the samples. A transmission electron microscopic survey of approximately 275 individual catalyst particles showed them to be generally cylindrical in shape with the following average dimensions: Co, 19 nm diameter × 38 nm long; Ni, 21 nm diameter × 32.1 nm long; Fe, 15 nm diameter × 22.0 nm long. Catalyst particle lengths varied widely, from approximately 7 to 458 nm long. Profiles and rates for the cobalt generated nanotubes are similar in both cases, showing peak oxidation rate in the vicinity of 480 °C, as well as a lesser peak at approximately 860 °C (Figure 9, bottom, and Figure 10, bottom). Nickel generated nanotubes show a slightly higher temperature associated with the maximum oxidation rate when synthesized using the spray pyrolysis method and a $NiCl_2$ catalyst precursor (maximum rate at 579 °C) than when synthesized using the low-flow method and a nickelocene precursor (maximum rate at 562 °C). A very small peak is observed at approximately 860 °C for the nickel spray pyrolysis sample as well. The case of ferrocene generated nanotubes is more significantly different for the two synthesis methods. In the low-flow synthesis case, the maximum rate of oxidation occurs at approximately 590 °C, whereas the spray pyrolysis sample exhibits maximum burnoff at roughly 537 °C. Possible reasons behind this observation will be discussed later.

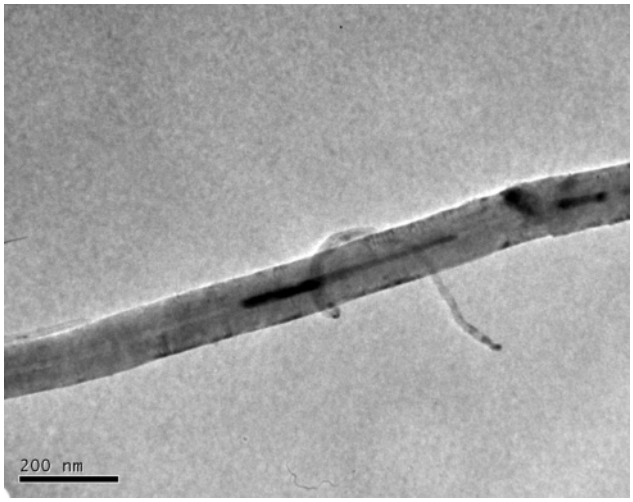

Figure 3. A pair of individual nanotubes, representative of size variations observed. Catalyst particles are evident at the center and right side of the large nanotube and at the lower right end of the smaller nanotube. Scale bar = 200 nm.

Finally, Raman spectroscopy was performed on samples with varied synthesis temperatures and varied catalyst types to ascertain whether the observed burnoff curve changes were a result of structural defects in the nanotubes; these results appear in Figure 11. Spectra were recorded at several different locations on the nanotube samples, normalized, and averaged to have a more accurate representation of the sample bulk.

Discussion

The first signs of mass loss in the graphite/catalyst mixture profiles occur in all samples at approximately the same point, close to 615 °C, below which all samples appear to be relatively

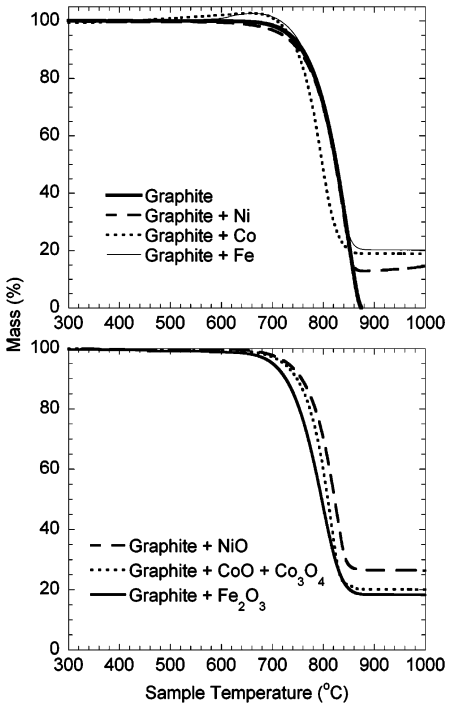

Figure 4. Mass-loss profiles for graphite and graphite−catalyst mixtures (top) and graphite−catalyst oxide mixtures (bottom). Cobalt, its oxide, and iron oxide show a marked impact on the oxidative stability of graphite.

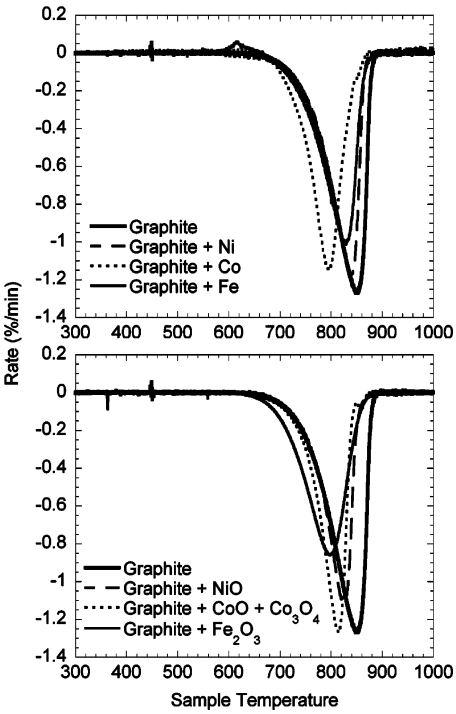

Figure 5. Oxidation rates derived from mass-loss profiles shown in Figure 4. Maximum graphite oxidation rates with Ni, Co, and Fe were observed at 800, 775, and 830 °C, respectively. Maximum rates with their oxides were observed at 805, 785, and 798 °C, respectively.

stable. From that point upward, however, the curves separate and follow different paths. Some variation in the temperature of maximum oxidation rate was observed, as noted previously, perhaps due to varying amounts of catalyst particles present or to distribution differences occurring through the imperfect mixing of the graphite and catalyst. In the samples tested, the remnant mass ranged from approximately 15 to 30 wt % of the original sample size. The curves shown in Figures 4 and 5 are

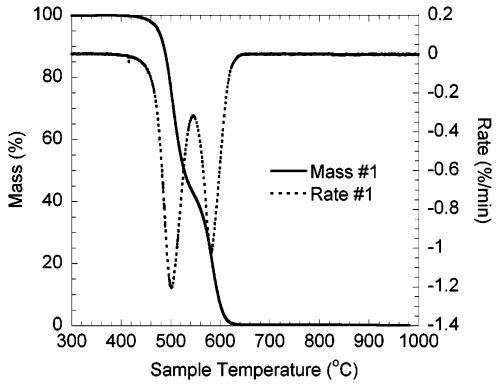

Figure 6. Mass-loss profile and rate of oxidation of an amorphous carbon/nanotube sample. Two oxidation rate peaks are observed at 500 and 581 °C, corresponding to amorphous carbon (approximately 55% by mass) and carbon nanotubes (45% mass).

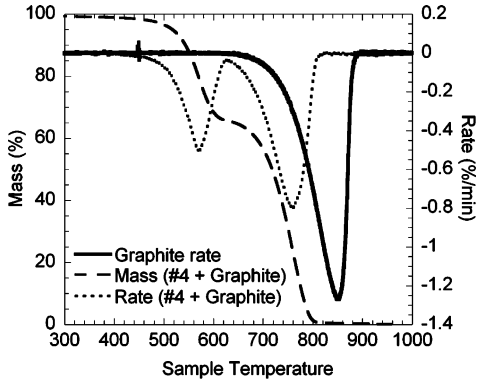

Figure 7. Mass-loss profile and rate of oxidation of MWNT mixed with high-purity graphite. A plateau in mass occurs at a point roughly corresponding to the original mixture ratio of nanotubes and graphite. Dual maxima in oxidation rate are observed at 570 and 760 °C, corresponding to the two forms of carbon.

generally representative and reflect approximately equal amounts of metal catalyst.

The presence of transition metals is known to catalyze the gasification of carbon,[21−23] but the mechanism by which the transition metal catalysts affect this is not fully understood. One theory[21] suggests that the metal particles form an intermediate, nonstoichiometric oxide and are then reduced through the oxidation of surrounding carbon particles. In this case, the catalytic effect of the metal particle would be partially dependent on the thermodynamics of oxidation and would thus vary from one element to another, suggesting a possible reason for the differences between the observed catalytic effects of each metal on the nanotubes. A detailed investigation of the actual mechanism of the catalytic effect is outside the scope of these experiments and is not covered here.

In the cases of elemental iron, nickel and nickel oxide, however, little change in the oxidation profile is observed. The burnoff profiles for these mixtures follow that of pure graphite before leveling off at a mass roughly corresponding to their initial mix ratios. The temperature of peak oxidation rate in each shows only minor variation from that of pure graphite, suggesting that they have minimal catalytic effect in the reaction. With such a small change between the profiles for pure graphite and these mixtures, it is reasonable to argue that no catalytic effect is observed, and that the temperature shift corresponding to peak burnoff reflects only the earlier slowing of the reaction due to the smaller relative amount of carbon.

In all cases where an elemental metal catalyst is present, a slight mass gain is apparent, arising from the initial oxidation

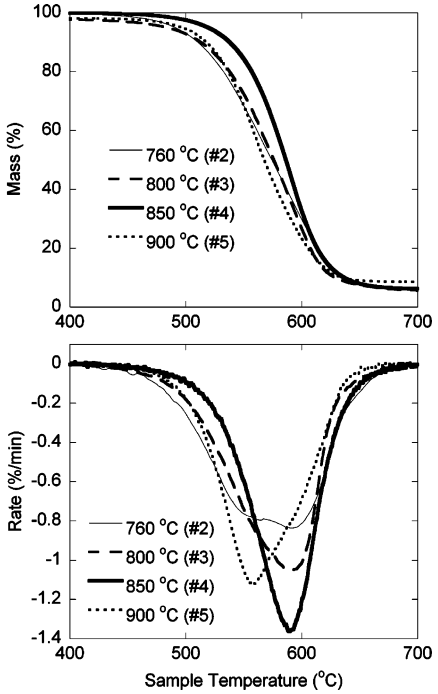

Figure 8. Effects of synthesis temperature on mass-loss profile (top) and oxidation rate (bottom). Peak stability versus oxidation is observed at 850 °C synthesis temperature, above and below which increased amounts of less stable forms of carbon are present.

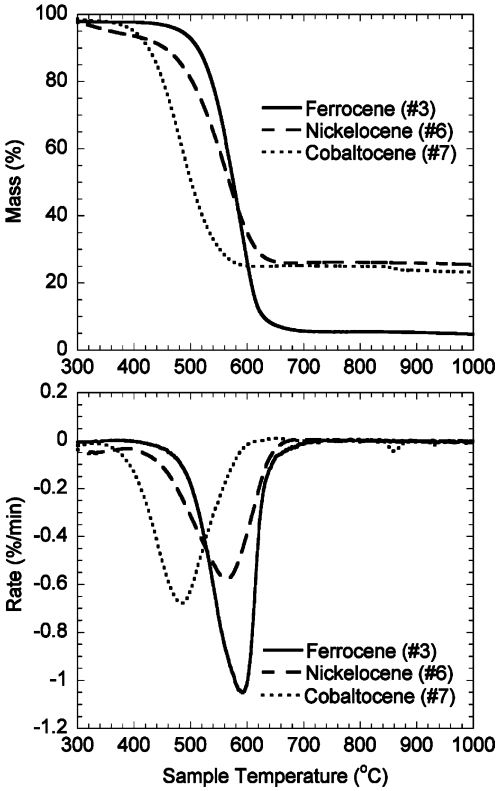

Figure 9. Catalyst effects on oxidation of low-flow generated nanotubes: mass profile (top) and rate (bottom). Cobalt generated nanotubes showed the lowest stability, followed by nickel and iron catalyzed nanotubes. A small oxidation rate peak associated with graphite was noted when cobalt catalysts were used.

of those metals. In each case, the oxidation of the metal begins before the oxidation of the carbon. Cobalt oxidation begins first, with mass gain beginning at 325 °C, followed by nickel and iron at 400 °C. Nickel oxidation appears to progress more

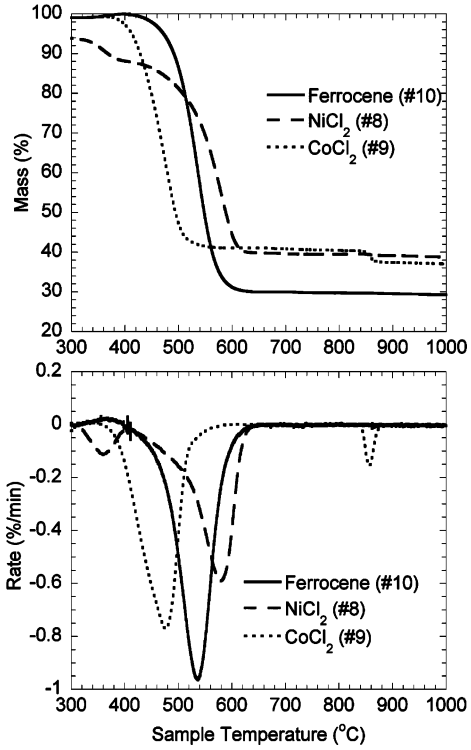

Figure 10. Catalyst effects on oxidation of spray pyrolysis generated nanotubes: mass profile (top) and rate (bottom). Cobalt generated nanotubes again showed the lowest stability, followed by iron, and then nickel catalysts. Graphite-related oxidation peaks were more pronounced with cobalt catalysts, but were also observed with nickel generated CNTs.

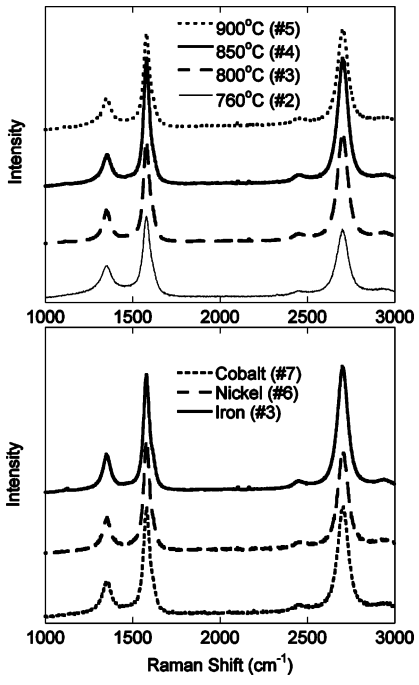

Figure 11. Raman spectra for samples with varying synthesis temperature (top, using an iron catalyst) and varying catalyst type (bottom, using a synthesis temperature of 800 °C). Spectra have been offset for ease of viewing features.

quickly than iron, showing a more rapid mass gain apparent in Figure 4. While these mass increases may be attributed to the partial oxidation of exposed catalyst particles, they are not large enough to reflect the complete oxidation of all catalyst particles in the sample. The end results of the oxidation are black cobalt oxides, green nickel oxide, or reddish iron oxide powder,

confirmed by XRD to be CoO and Co_3O_4, NiO, or Fe_2O_3, respectively, suggesting the remaining catalyst particles oxidize simultaneously with the graphite, and are thus not distinct in the mass-loss curve.

The catalytic effects of iron oxide, cobalt, and cobalt oxides are quite evident in both the burnoff profiles and their corresponding rate curves. Of particular note is the difference in burnoff profiles between graphite with elemental iron and graphite with Fe_2O_3. The strong catalytic effect of Fe_2O_3 compared to the nearly negligible one of elemental iron contradicts the behaviors predicted by the intermediate composition catalytic mechanism theory, which implies that both would have equivalent catalytic activity. If iron and its oxide differ in catalytic activity, the data suggest that elemental iron does not form an oxide early enough in the process to significantly impact the graphite gasification, but completes its transition to Fe_2O_3 once the graphite oxidation reaction has reached an active state.

Figures 6 and 7 clearly show the separation by reactivities of differing forms of carbon. Amorphous, nanotube, and graphitic carbons show peak oxidation rates at increasing temperatures. The distinct burnoff peaks confirm the potential for oxidative separation of the carbon forms and allow for the visual separation of nanotubes from other forms of carbon in TGA profiles. Biphenyl, a synthesis byproduct, was also analyzed by TGA (see Supporting Information) and was found to burn off at a low enough temperature (peak oxidation rate at 222 °C) that it did not impact the profiles observed for other forms of carbon.

The nanotubes used in this study show a decreased stability with respect to graphite, as has been observed previously,[7] but contrary to observations elsewhere.[8,20] The catalytic effect of Fe_2O_3 (from the nanotube synthesis catalyst) upon graphite is also observed in Figure 7, reducing the peak oxidation rate temperature from that of pure graphite. The synthesis catalyst particles are encapsulated within the nanotubes and are thus shielded from oxygen and oxidation until the tubes are opened or consumed. As such, one would expect a slight delay in the profile before the catalytic effects could be observed. Mössbauer analysis determines their forms as elemental iron (32%), Fe_3C (37%), austenite (28%), and a small amount of Fe^{3+} (2%). As the nanotubes are consumed, these forms of iron are oxidized to Fe_2O_3, which may then catalyze the oxidation of the remaining nanotubes as well as the graphite. This in turn lowers the temperature of the maximum graphite burnoff rate from 850 °C to approximately 760 °C, an even more pronounced effect than that observed by mixing Fe_2O_3 and graphite directly (peak rate at 800 °C, Figure 5). Despite any delay due to the carbon encapsulation of the growth catalyzing iron, this is to be expected given the much smaller size of the resultant oxidized nanoparticles, which possess a greater specific surface area, allowing for increased surface interactions and a faster overall reaction.

CNT samples synthesized with differing furnace temperatures show increasing stability with respect to thermal oxidation as synthesis temperature increases to 850 °C, after which stability appears to decrease. Hornyak et al. showed[24] that CVD nanotube synthesis will not proceed above a certain temperature, so a temperature of maximum stability for a set of synthesis conditions is expected, above which stability will decrease as amorphous carbon deposits and nanotube defect sites increase. The 900 °C synthesis sample confirms this, showing a decrease in temperature of the maximum burnoff rate. Examination of Figure 8 reveals dual peaks in the rate curve at approximately 560 and 595 °C. As the synthesis temperature increases up to an optimum point, the majority of burnoff shifts into the higher temperature peak, indicating increased formation of more stable or less defected nanotubes. The 900 °C curve surpasses this point and a rapid return to formation of structures associated with the lower peak is observed. In each case, the reaction appears to terminate at approximately the same point.

The Raman spectra shown in the top of Figure 11 support this idea of an optimal synthesis temperature. Raman spectroscopy performed on multiwalled nanotubes generally results in a characteristic fingerprint: the D band, which appears at approximately 1350 cm^{-1}, is associated with disordering in the nanotube,[25] while the G band appears at approximately 1580 cm^{-1}, a result of sp^2 hybridized carbon bonding (the in-plane stretching mode for graphene sheets). The G′ band is the second-order harmonic of the D band and appears in the realm of 2700 cm^{-1}. The G and D bands are frequently compared to provide an idea of the structural quality of a nanotube sample,[26,27] but it has also been suggested that a more accurate quality characterization may be obtained through comparison of the G′ and D bands. Spectra for ideal nanotubes would reflect high G:D or G′:D peak ratios. G:D ratios for synthesis temperatures of 760, 800, 850, and 900 °C were measured as 2.21, 2.89, 3.60, and 2.76, respectively. G′:D ratios were measured at the same temperatures as 1.99, 3.08, 3.61, and 2.91, respectively. For the temperatures examined, both peak ratios increase with increasing temperature up to 850 °C, suggesting a decrease in structural defects, but then the peak ratios decrease slightly again at 900 °C.

When comparing Figures 5 and 7, it becomes apparent that the behavior of the iron and graphite in each system differs. In Figure 5, it appears that the iron does not noticeably catalyze the oxidation of the graphite. In Figure 7, however, a large shift in the burnoff temperature of graphite is observed. It appears that the oxidation of the nanotube structures may catalyze the oxidation of the contained iron or iron carbide nanoparticles, thereby bringing the catalytic role of Fe_2O_3 into the reaction earlier and at a lower temperature than was observed in Figure 5. It is also possible that the presence of iron carbides changes the reaction sufficiently to either catalyze the oxidation itself or to generate the Fe_2O_3 at a lower temperature, allowing the catalyzed oxidation of graphite.

When varying catalyst types, it was found that the mass-loss and oxidation rate curves were largely insensitive to catalyst precursor composition, but depended primarily on the actual catalyst metal used. For example, little variation in the burnoff profile was observed between nanotubes generated with nickelocene and $NiCl_2$ catalysts, but large variations were observed between those generated with $NiCl_2$ and $CoCl_2$ catalysts.

Synthesis method appeared to play a role in the stability of some nanotubes investigated. When a cobalt catalyst was used, no significant change was noted between the low-flow and spray pyrolysis conditions. However, when either a nickel or ferrocene catalyst was used, a shift was observed. Nickel catalysts showed an increase in the temperature of maximum oxidation rate (approximately 17 °C) for the spray pyrolysis method, where the iron catalysts showed a decrease of approximately 53 °C. While a 17 °C change is inconclusive, the 53 °C shift present in the iron catalyzed nanotubes suggests a nontrivial change in their defect density. Since the primary difference between the two methods is the reagents' dwell time within the furnace, it is possible that nascent nanotube formation occurs at a lower temperature due to the nanotubes' higher velocity through the furnace and slower heating rate and thus results in a higher defect density. That this effect is not observed when other

catalysts are used suggests that their optimal synthesis temperatures may be lower than that for iron catalysts.

Of the samples tested, cobalt generated nanotubes consistently burned off most quickly, matching the behavior demonstrated in the catalyst−graphite mixtures. In both the low-flow and spray pyrolysis generated cobalt tubes, the profiles show the primary burnoff of the nanotubes, but also reflect a secondary burnoff peak at approximately 860 °C. A similar, but much smaller oxidation peak is observed at the same temperature for the nickel catalyzed spray pyrolysis nanotubes. This peak corresponds to the temperature at which pure graphite was observed to oxidize, suggesting these catalysts may also assist the formation of graphite particles under the given synthesis conditions. Should these graphite particles remain free or isolated from the catalyst particles, they could account for these burnoff peaks. No signs of graphite were found in other nanotube samples, except for those where graphite was manually introduced.

With the exception of the ferrocene catalyzed spray pyrolysis nanotubes, as noted above, oxidation of the various catalyst-grown nanotubes follows the trends observed in the graphite/catalyst mixtures. Cobalt catalyzed carbon nanotubes show the lowest stability relative to oxidation, followed by nickel and iron grown nanotubes with comparable stability. By comparison with Saxby et al.,[20] it is evident that each of the nanotubes tested exhibits an increased oxidative stability relative to amorphous carbon and C_{60}, but decreased relative to that of diamond.

Raman analyses of these samples show that the change in burnoff temperature is not a consequence of structural defects in the nanotubes. G:D band ratios are comparable for all three catalyst types−2.89 for iron, 2.78 for nickel, and 2.79 for cobalt (Figure 11, bottom)−suggesting that the observed phenomena must be a result of the included catalyst type. G′:D ratios show more variation, however: Fe, 3.08; Ni, 2.57; Co, 2.75. This latter set of results suggests that the differences between the nickel and iron curves may be a result of structural defects, but that the mass-loss curve associated with the cobalt catalyst definitely reflects a strong catalytic effect.

As a direct result of the differences in oxidation resistance discussed above, the specific circumstances of application of the nanotubes should be considered when determining what catalyst to use in their synthesis. In applications subjecting nanotubes to high temperatures or oxidation, or where nanotubes are utilized in critical ways, an engineer should determine whether the degree of oxidation susceptibility corresponding to the use of a catalyst will compromise the nanotube over the life of the application.

As reported elsewhere,[6] the nanotubes show a high resistance to oxidation until a critical temperature is reached, which appears to depend, in part, on the catalyst used in the nanotube synthesis and, at least in the case of CVD grown CNTs, the synthesis temperature. Nickel and iron generated nanotubes showed relative stability until approximately 450 °C, while cobalt generated nanotubes appeared stable to approximately 400 °C. Of course, oxidation commences at a lower temperature, but at rates slow enough that it was not measurable in the time scale of these scans. Competitive oxidation always takes place among different types of carbon, but will proceed at different rates, as has been demonstrated.

The mass-loss profile shown for low-flow, ferrocene generated nanotubes is similar to that for the raw multiwalled nanotubes examined by Bom et al.,[7] with the maximum mass loss for the present sample occurring at approximately 595 °C, compared to approximately 575 °C for xylene/ferrocene tubes in Bom et al. Notably different is the nanotube mass-loss profile given by Pang et al.,[8] which shows a maximum rate of mass loss at approximately 695 °C, a full 100 °C higher, with no catalyst used.

Different oxidation behaviors between laser-ablation-generated and arc-discharge-generated nanotubes have been reported previously.[11] The current nanotubes, as well as those used by Bom et al.,[7] were fabricated through chemical vapor deposition, whereas those analyzed by Pang et al.[8] were produced through arc-discharge synthesis. The presence of an electric field during synthesis, such as that present in the arc-discharge method and generally lacking in standard chemical vapor deposition, has been shown[28,29] to help stabilize the formation of carbon nanotubes. Similarly, higher temperatures present during synthesis allow the annealing out of defects as the nanotubes are formed. Given the comparatively low temperatures used in CVD synthesis (versus those present in laser-ablation or arc-deposition methods) and lack of electric fields to assist formation, nanotubes created in this manner will exhibit a higher defect density, thereby resulting in lower burnoff temperatures.[7] Further, the present work demonstrates the potential for catalyzed oxidation by the growth catalyst, which could result in even lower burnoff temperatures. With these considerations in mind, the large temperature difference observed between the CNTs of Pang et al., Bom et al., and the present study can be rationalized.

Conclusions

Synthesis conditions and their resulting effects on CNT structure and stability have been examined, and the synthesis and analysis of each sample have been replicated with little variation, except as noted. Carbon nanotubes of comparable crystalline defect density have been synthesized with each of the catalysts examined utilizing the low-flow method. Iron oxide, cobalt oxide, and cobalt catalysts have been shown to have a significant depressing effect on the oxidative stability of the nanotubes tested while iron, nickel, and nickel oxide do not appear to significantly reduce the stability of nanotubes in their presence with the noted exception of iron in spray pyrolysis generated nanotubes. Carrier gas flow rates were compared and found to produce nanotubes of generally comparable stability with nickel and cobalt catalysts, but significant variation was observed when using iron. Nanotube synthesis temperature was found to have a small but measurable effect on structure, with an optimal temperature found to be in the region of 850 °C for ferrocene catalyzed tubes. This analysis provides an upper limit to the window for the oxidative purification of CVD generated nanotubes and exhibits the significant impact that a catalyst may have on the oxidative stability.

Acknowledgment. The authors thank Christian Deck and Ralf Brunner for their previous work and guidance, Fred Parker for help with Mössbauer analysis, and Jason Flowers for assistance with thermogravimetric analysis. G.S.B.M. acknowledges the financial support of the Jacobs Fellowship from the Jacobs School of Engineering at UC San Diego.

Supporting Information Available: Figures showing the mass-loss profiles for a given sample at varying temperature ramp rates and biphenyl sludge byproduct. This material is available free of charge via the Internet at http://pubs.acs.org.

References and Notes

(1) Iijima, S. *Nature* **1991**, *354*, 56.

(2) Liu, C.; Fan, Y. Y.; Liu, M.; Cong, H. T.; Cheng, H. M.; Dresselhaus, M. S. *Science* **1999**, *286*, 1127.

(3) Schadler, L. S.; Giannaris, S. C.; Ajayan, P. M. *Appl. Phys. Lett.* **1998**, *73*, 3842.

(4) Dillon, A. C.; Jones, K. M.; Bekkedahl, T. A.; Kiang, C. H.; Bethune, D. S.; Heben, M. J. *Nature* **1997**, *386*, 377.

(5) White, C. T.; Todorov, T. N. *Nature (London)* **1998**, *393*, 240.

(6) Ajayan, P. M.; Ebbesen, T. W.; Ichihashi, T.; Iijima, S.; Tanigaki, K.; Hiura, H. *Nature* **1993**, *362*, 522.

(7) Bom, D.; Andrews, R.; Jacques, D.; Anthony, J.; Chen, B.; Meier, M. S.; Selegue, J. P. *Nano Lett.* **2002**, *2*, 615.

(8) Pang, L. S. K.; Saxby, J. D.; Chatfield, S. P. *J. Phys. Chem.* **1993**, *97*, 6941.

(9) Rinzler, A. G.; Liu, J.; Dai, H.; Nikolaev, P.; Huffman, C. B.; Rodriguez-Macias, F. J.; Boul, P. J.; Lu, A. H.; Heymann, D.; Colbert, D. T.; Lee, R. S.; Fischer, J. E.; Rao, A. M.; Eklund, P. C.; Smalley, R. E. *Appl. Phys. A (Mater. Sci. Process.)* **1998**, *67*, 29.

(10) Chiang, I. W.; Brinson, B. E.; Huang, A. Y.; Willis, P. A.; Bronikowski, M. J.; Margrave, J. L.; Smalley, R. E.; Hauge, R. H. *J. Phys. Chem. B* **2001**, *105*, 8297.

(11) Dillon, A.; Landry, M.; Jones, K.; Webb, J.; Heben, M. J. The Oxidation and Reduction of Single-Wall Carbon Nanotube Materials. Presented at the Symposium on Recent Advances in the Chemistry and Physics of Fullerenes and Related Materials, 1997, Montreal, Quebec, Canada.

(12) Lozano, K.; Files, B.; Rodriguez-Macias, F. J.; Barrera, E. V. Purification and functionalization of vapor grown carbon nanotubes and single wall nanotubes. In Powder Materials: Current Research and Industrial Practices. Proceedings of Symposium. Held during 1999 TMS Fall Meeting. *TMS*—Miner. Met. Mater. Soc. **1999**, 333−340.

(13) Martinez, M. T.; Callejas, M. A.; Benito, A. M.; Cochet, M.; Seeger, T.; Anson, A.; Schreiber, J.; Gordon, C.; Marhic, C.; Chauvet, O.; Maser, W. K. *Nanotechnology* **2003**, *14*, 691.

(14) Park, Y. S.; Choi, Y. C.; Kim, K. S.; Chung, D. C.; Bae, D. J.; An, K. H.; Lim, S. C.; Zhu, X. Y.; Lee, Y. H. *Carbon* **2001**, *39*, 655.

(15) Ajayan, P. M.; Iijima, S. *Nature* **1993**, *361*, 333.

(16) Tsang, S.; Chen, Y.; Harris, P.; Green, M. *Nature* **1994**, *372*, 159.

(17) Zhang, X.; Cao, A.; Sun, Q.; Xu, C.; Wu, D. *Mater. Trans.* **2002**, *43*, 1707.

(18) Ajayan, P. M.; Stephan, O.; Redlich, P.; Colliex, C. *Nature* **1995**, *375*, 564.

(19) Tsang, S. C.; Harris, P. J. F.; Green, M. L. H. *Nature* **1993**, *362*, 520.

(20) Saxby, J. D.; Chatfield, S. P.; Palmisano, A. J.; Vassallo, A. M.; Wilson, M. A.; Pang, L. S. K. *J. Phys. Chem.* **1992**, *96*, 17.

(21) Thomas, J. M. Microscopic Studies of Graphite Oxidation. In *Chemistry and Physics of Carbon*; Walker, P. L., Ed.; Marcel Dekker: New York, 1965; Vol. 1, p 121.

(22) Kelemen, S. R. *Appl. Surf. Sci.* **1987**, *28*, 439.

(23) Pan, Z. J.; Yang, R. T. *J. Catal.* **1991**, *130*, 161.

(24) Hornyak, G. L.; Grigorian, L.; Dillon, A. C.; Parilla, P. A.; Jones, K. M.; Heben, M. J. *J. Phys. Chem. B* **2002**, *106*, 2821.

(25) Dresselhaus, M. S.; Dresselhaus, G.; Jorio, A.; Souza Filho, A. G.; Saito, R. *Carbon* **2002**, *40*, 2043.

(26) Bacsa, W. S.; Ugarte, D.; Chatelain, A.; de Heer, W. A. *Phys. Rev. B* **1994**, *50*, 15473.

(27) Tohji, K.; Goto, T.; Takahashi, H.; Shinoda, Y.; Shimizu, N.; Jeyadevan, B.; Matsuoka, I.; Saito, Y.; Kasuya, A.; Ohsuna, T.; Hiraga, K.; Nisshina, Y. *Nature (London)* **1996**, *383*, 679.

(28) Maiti, A.; Brabec, C. J.; Roland, C. M.; Bernholc, J. *Phys. Rev. Lett.* **1994**, *73*, 2468.

(29) Lou, L.; Nordlander, P.; Smalley, R. *Phys. Rev. B* **1995**, *52*, 1429.